

Resolution enhancement of $\bar{p}\text{He}^+$ atomic line profiles measured with a pulsed dye laser and a Fizeau wavelength meter

Masaki Hori

CERN, CH-1211 Geneva 23, Switzerland

Ryugo S. Hayano and Eberhard Widmann

Department of Physics, University of Tokyo, Hongo, Bunkyo-ku, Tokyo 113-0033, Japan

Hiroyuki A. Torii

Institute of Physics, University of Tokyo, Komaba, Meguro-ku, Tokyo 153-8902, Japan

Received July 31, 2003

A Fizeau wavelength meter was used to compensate for fluctuations in the longitudinal mode structure and wavelength of a pulsed dye laser. The average laser linewidth was effectively narrowed by selection of laser pulses with a single longitudinal mode. These techniques were recently employed to measure some atomic transition wavelengths in $\bar{p}\text{He}^+$ to fractional precisions greater than 1 part in 10^7 . The wavelengths were absolutely calibrated against iodine or tellurium lines by absorption spectroscopy or against neon or argon lines by optogalvanic spectroscopy. © 2003 Optical Society of America

OCIS codes: 300.6360, 300.6210, 120.0120, 120.3180, 140.3600.

We describe a technique whereby the linewidth of a pulsed dye laser is effectively narrowed by use of a Fizeau wavelength meter,¹⁻³ which enables laser spectroscopy experiments to yield results with accuracies of better than 1 part in 10^7 . Some transition wavelengths in antiprotonic helium ($\bar{p}\text{He}^+ \equiv e^- - \bar{p} - \text{He}^{2+}$) atoms of $\lambda = 264\text{--}726$ nm were recently measured by this method.^{4,5} These experiments, carried out at CERN's Antiproton Decelerator, led to a 1×10^{-8} limit on any differences between the masses and the charges of antiprotons and protons. The method also allowed us to resolve the hyperfine structure in these optical transitions that arises from magnetic interactions between antiprotons and electrons and to measure the atom's magnetic transition frequencies in a laser-microwave resonance experiment.⁶

In these experiments (Fig. 1), dye lasers (Lambda Physik Scanmate-2E) were pumped by the second or third harmonic of a Nd:YAG laser (Coherent Infinity), thereby producing 4–6-ns-long laser pulses with wavelengths of $\lambda = 463\text{--}746$ nm and energies of $E = 1\text{--}20$ mJ. To probe UV transitions at $\lambda = 264\text{--}373$ nm we frequency doubled the dye laser in a beta barium borate (BBO) crystal. The 30-cm-long dye laser cavity⁷ contained a Littrow-mounted grating (full width at half-maximum bandwidth, $\Gamma \sim 6$ GHz) and an intracavity etalon ($\Gamma \sim 1.2$ GHz), such that three longitudinal cavity modes spaced by frequency intervals of $\Delta\nu = 0.5$ GHz coexisted in the laser's gain envelope. Similar lasers are widely used in experiments involving precisions of $\sim 10^{-6}$. Measurements with Fizeau interferometers^{8,9} have shown that the laser wavelengths and the longitudinal mode intensities fluctuate from pulse to pulse, imposing serious limits on this precision. These quantum fluctuations

arise because it is the first few photons, emitted spontaneously from the dye and proceeding to occupy the multiple cavity modes, that initiate the lasing process. The number of initial photons in a given mode thus fluctuates from pulse to pulse, following an exponential probability distribution.¹⁰ The resultant laser pulse can make only a few round trips in the cavity during its nanosecond-scale duration, so a

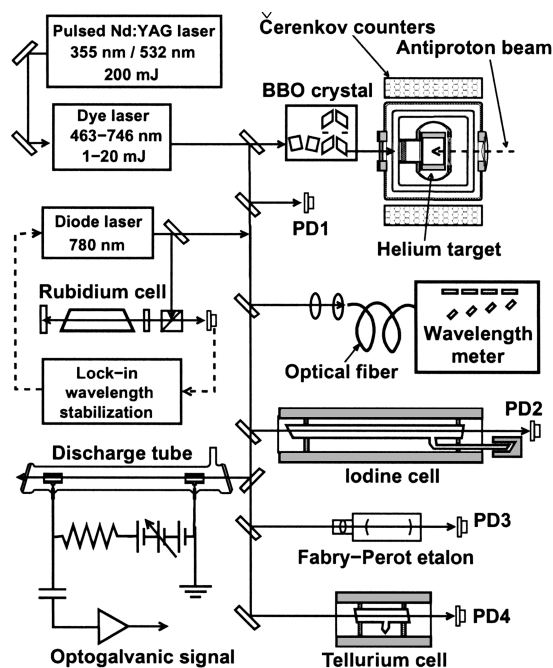


Fig. 1. Experimental setup for high-precision laser spectroscopy of $\bar{p}\text{He}^+$: PDs, photodiodes.

single mode usually cannot dominate and quench the others. We found, however, that a fraction of these laser pulses is in fact single mode, as described below.

The wavelength meter (Cluster LambdaMeter LM-007) used here contained four Fizeau interferometers of various free spectral ranges (FSRs), which were embedded in a thermostabilized monolithic quartz block filled with neon gas. The laser beams were spatially filtered with a single-mode optical fiber before they entered the instrument. The interference patterns produced by individual laser pulses were recorded, and the wavelengths were determined from the positions of the fringes and from the relative intervals between them. The longest interferometer had a FSR of $\Delta\nu = 3.8$ GHz and a finesse of $F \sim 10$. We estimated the latter value by measuring the fringes produced by an external-cavity cw diode laser of linewidth $\Gamma < 1$ MHz. To monitor and correct any long-term drifts in the readings of the wavelength meter, we locked the cw laser wavelength to the hyperfine components of the ^{85}Rb transition $5^2S_{1/2} \rightarrow 5^2P_{3/2}$ at $\lambda = 780.2$ nm by Doppler-free, frequency-modulated saturation spectroscopy.¹¹ The readings shifted by ± 15 MHz over a 10-h period.

In Fig. 2(a) the fringe pattern of a 3.8-GHz FSR interferometer irradiated with ten consecutive dye laser pulses at $\lambda = 726.1$ nm is shown. Most of the fringes were broad, with a microstructure of two or three peaks separated by intervals of $\Delta\nu = 0.5$ GHz, indicating a multimode laser beam. In approximately 20–30% of the cases, however, the fringes showed that nearly all the energy happened to be concentrated in a single longitudinal mode; the example presented in Fig. 2(b) implies a laser linewidth of $\Gamma \sim 0.4$ GHz (after deconvolution of the 0.4-GHz resolution of the interferometer). In Fig. 2(c), fringes that correspond to the intensity-normalized summation of 100 laser pulses fired at a repetition rate of $f = 10$ Hz are shown. Owing to fluctuations of 0.3–0.8 and 0.4–1.8 GHz, respectively, in the laser wavelength and linewidth, the time-averaged linewidth was large ($\Gamma \sim 1.0$ GHz). This linewidth size limited the resolution of conventional laser spectroscopy experiments wherein the measured signals were integrated over many laser pulses, e.g., by use of a boxcar integrator. In the measurements described below, we effectively narrowed this linewidth to $\Gamma = 0.4$ –0.5 GHz by (i) detecting the spectroscopic signals and fringes produced by each laser pulse, (ii) rejecting laser pulses that deviated from a single-mode structure, and (iii) determining the laser wavelength.

Laser spectroscopy of $\bar{p}\text{He}^+$ was carried out in the following way⁴: Every 100 s, a pulse containing $\sim 10^7$ antiprotons was stopped in a helium target, thereby producing $\sim 10^6$ metastable $\bar{p}\text{He}^+$ atoms [i.e., atoms in which the antiprotons populate states with large principal ($n \sim 38$) and angular-momentum ($l \sim n$) quantum numbers that have radiative lifetimes $\tau \geq 1$ μs]. These atoms were irradiated with a laser pulse of energy density $\Theta = 0.1$ –1 mJ/cm^2 , which stimulated atomic transitions to short-lived states that proceeded rapidly to antiproton annihilation in the nucleus. Charged pions emerging from these

annihilations (measured by a Čerenkov detector) signaled the resonance condition between the laser and the atom. In Fig. 3(a) the resonance profile of the $\bar{p}\text{He}^+$ transition ($n, l = (39, 35) \rightarrow (38, 34)$) at $\lambda = 597.3$ nm is shown; each data point represents the average of two antiproton pulses.

During the intervals between antiproton arrivals we calibrated the wavelength meter by carrying out Doppler-broadened absorption spectroscopy of the rovibrational transition lines of molecular iodine¹² (relevant wavelengths, $\lambda = 525$ –746 nm) or tellurium¹³ (463–471 nm). We measured iodine transitions at $\lambda = 525$ –598 nm by filling a 70-cm-long, 1.5-cm-diameter

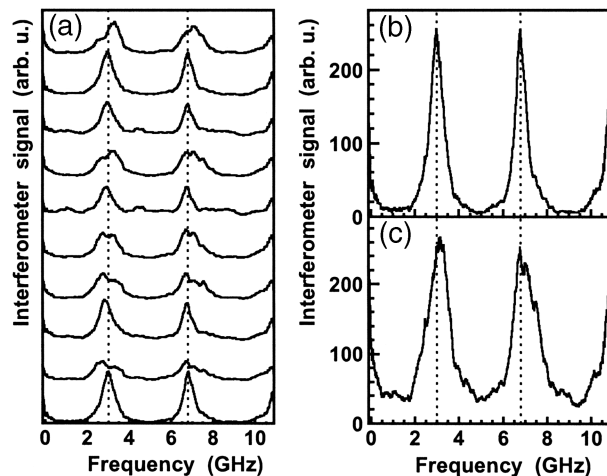


Fig. 2. (a) Fringe patterns of a Fizeau interferometer with a free spectral range of $f = 3.8$ GHz irradiated by ten consecutive dye laser pulses. (b) Fringes produced by a dye laser pulse with a single longitudinal mode. (c) Summation of the fringe patterns produced by 100 laser pulses fired at a repetition rate of $f = 10$ Hz.

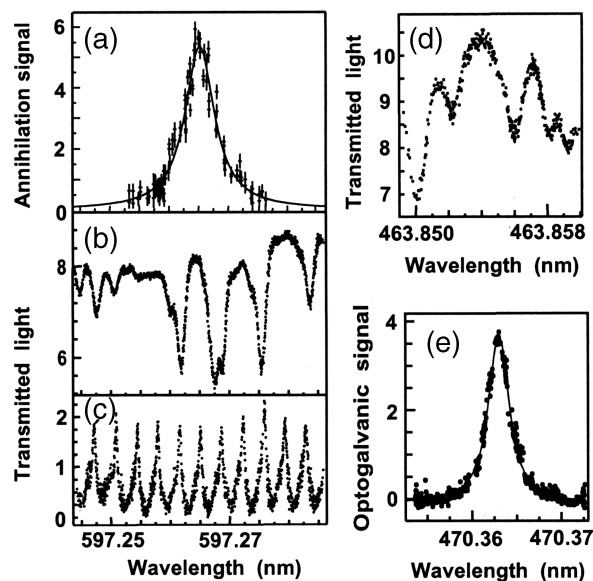


Fig. 3. (a) Resonance profile of the $\bar{p}\text{He}^+$ transition ($n, l = (39, 35) \rightarrow (38, 34)$), (b) iodine absorption spectrum, (c) transmission fringes of a Fabry–Perot etalon measured simultaneously. (d) Absorption spectrum of tellurium and (e) optogalvanic spectrum of argon. All signal intensities are plotted in arbitrary units.

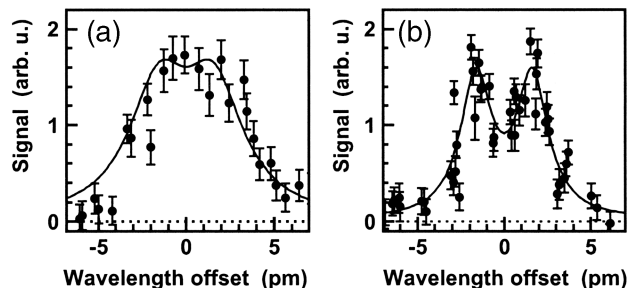


Fig. 4. Resonance profile of the $\bar{p}^4\text{He}^+$ transition $(n, l) = (37, 35) \rightarrow (38, 34)$ at $\lambda = 726.1$ nm, measured (a) without and (b) with the wavelength meter correcting the wavelength fluctuations and narrowing the laser linewidth.

glass cell with pure $^{127}\text{I}_2$ (Fig. 1) and heating it to $T = 150\text{--}250^\circ\text{C}$ to populate the associated states. The corresponding temperatures that we used to measure transition wavelengths $\lambda = 611\text{--}673$ and $\lambda = 713\text{--}746$ nm (involving highly excited states) were $T = 300\text{--}500$ and $T = 600\text{--}650^\circ\text{C}$, respectively. Part of the cell was maintained at $T = 25\text{--}50^\circ\text{C}$ to regulate the iodine pressure to $P = 40\text{--}300$ Pa. Laser pulses with energy density $\Theta \sim 1 \mu\text{J}/\text{cm}^2$ and repetition rate $f = 5$ Hz were passed through the cell, and the transmitted intensity of each of these pulses was measured by photodiode PD2 read out by a charge-sensitive analog-to-digital converter (LeCroy 2249A). The signal was normalized to the laser energy measured by photodiode PD1. In Fig. 3(b) an iodine spectrum measured simultaneously with the $\bar{p}^4\text{He}^+$ transition is shown; the $^{127}\text{I}_2$ line $(J, v) = (114, 14) \rightarrow (115, 2)$ at a known 12 wavelength of $\lambda = 597.261257(4)$ nm of the peak centroid was used for calibration. In Fig. 3(c) the transmission fringes of a confocal Fabry–Perot etalon with a FSR of $\Delta\nu = 3$ GHz, measured simultaneously by photodiode PD3, are shown. In Fig. 3(d) the transition of $^{130}\text{Te}_2$ at $\lambda = 463$ nm measured at a cell temperature $T = 600^\circ\text{C}$ in a similar way by photodiode PD4 is presented. The precision and reproducibility of the peak centroids in all these measurements were ± 20 MHz in the best case.

We carried out optogalvanic spectroscopy of neon¹⁴ and argon¹⁵ to calibrate some $\bar{p}\text{He}^+$ wavelengths. A glass cell, containing two 3-cm-long cylindrical electrodes with inner diameters of $d = 1.5$ cm made from iron (Fig. 1), was filled with neon or argon gas at a pressure of $P = 100$ Pa. The electrodes were axially aligned and suspended at a distance of $l = 30$ cm from each other, and a 50-mA electrical discharge was induced between them. Laser pulses of energy density $\Theta = 50 \mu\text{J}/\text{cm}^2$ were fired along the discharge. The resultant optogalvanic signals were detected through a decoupling condenser connected to the anode electrode, and their amplitudes were measured by a charge-sensitive amplifier and an analog-to-digital converter. The spectrum of the Ar–I transition $3s^23p^5(^2P_{1/2}^o)4s - 3s^23p^5(^2P_{3/2}^o)5p$ at $\lambda = 470.36317(3)$ nm (Ref. 15) thus measured is shown in Fig. 3(e). As a consistency check, we compared

several measured wavelengths of neon and argon at $\lambda = 463\text{--}746$ nm against those of iodine or tellurium that typically lie within 2 GHz of one another. The results indicate a calibration accuracy of 20–50 MHz.

Finally, we demonstrate the effectiveness of the present method in improving spectral resolution. In Fig. 4(a) the profile of the $\bar{p}^4\text{He}^+$ transition $(37, 35) \rightarrow (38, 34)$ at $\lambda = 726.1$ nm is shown. The plotted wavelengths represent the time-averaged readings of the wavelength meter [see Fig. 2(c)] over many laser pulses. The resolution was limited by the average laser linewidth. By comparison, we obtained the spectrum in Fig. 4(b) by measuring the wavelengths of individual laser pulses and discriminating those with linewidths of $\Gamma > 0.6$ GHz. The resolution was thus improved by a factor of ~ 3 . Two peaks separated by an interval of $\Delta\nu = 1.8$ GHz can now be seen; this configuration corresponds to the atom's hyperfine structure.

We acknowledge assistance from the Atomic Spectroscopy and Collisions Using Slow Antiprotons experiment at CERN and from N. Morita. This study was supported by the Grant-in-Aid for Creative Basic Research (10NP0101) of the Monbukagakusho. M. Hori's e-mail address is masaki.hori@cern.ch.

References

1. L.-S. Lee and A. L. Schawlow, *Opt. Lett.* **6**, 610 (1981).
2. C. Reiser, P. Esherick, and R. B. Lopert, *Opt. Lett.* **13**, 981 (1988).
3. P. S. Bhatia, C. W. McCluskey, and J. W. Keto, *Appl. Opt.* **38**, 2486 (1999).
4. M. Hori, J. Eades, R. S. Hayano, T. Ishikawa, J. Sakaguchi, E. Widmann, H. Yamaguchi, H. A. Torii, B. Juhász, D. Horváth, and T. Yamazaki, *Phys. Rev. Lett.* **87**, 093401 (2001).
5. M. Hori, J. Eades, R. S. Hayano, T. Ishikawa, W. Pirkel, E. Widmann, H. Yamaguchi, H. A. Torii, B. Juhász, D. Horváth, and T. Yamazaki, *Phys. Rev. Lett.* **91**, 123401 (2003).
6. E. Widmann, J. Eades, T. Ishikawa, J. Sakaguchi, T. Tasaki, H. Yamaguchi, R. S. Hayano, M. Hori, H. A. Torii, B. Juhász, D. Horváth, and T. Yamazaki, *Phys. Rev. Lett.* **89**, 243402 (2002).
7. T. W. Hänsch, *Appl. Opt.* **11**, 895 (1972).
8. L. A. Westling, M. G. Raymer, and J. J. Snyder, *J. Opt. Soc. Am. B* **1**, 150 (1984).
9. T. T. Kajava, H. M. Lauranto, and R. R. E. Salomaa, *Appl. Opt.* **31**, 6987 (1992).
10. V. R. Mironenko and V. I. Yudson, *Opt. Commun.* **34**, 397 (1980).
11. B. Bodermann, M. Klug, U. Winkelhoff, H. Knöckel, and E. Tiemann, *Eur. Phys. J. D* **11**, 213 (2000).
12. B. Bodermann, H. Knöckel, and E. Tiemann, *Eur. Phys. J. D* **19**, 31 (2002).
13. J. Cariou and P. Luc, *Atlas du Spectre d'Absorption de la Molécule de Tellure* (CNRS II, Orsay, France, 1980).
14. E. S. Chang, W. G. Schoenfeld, E. Biémont, P. Quinet, and P. Palmeri, *Phys. Scr.* **49**, 26 (1994).
15. W. Whaling, W. H. C. Anderson, M. T. Carle, J. W. Brault, and H. A. Zarem, *J. Res. Natl. Inst. Stand. Technol.* **107**, 149 (2002).